Analysis & Sensing

Research Article
doi.org/10.1002/anse.202500117

Chemistry Europe
European Chemical Societies Publishing

www.analysis-sensing.org

A Cost-Effective Hybrid Method For Homogeneous Matrix Coating in Matrix-Assisted Laser Desorption/Ionization Mass Spectrometry Imaging Using Simultaneous Spin and Spray Deposition

Lanaia Ítala Louzeiro Maciel, Jussara Valente Roque,* Almir Custodio Batista Junior, Gabriel Henry Morais Dufrayer, Naará da Silva Balbino, Keilah Valéria Naves Cavalcante, Marcos Divino Ferreira Junior, Andrea Rodrigues Chaves, and Boniek Gontijo Vaz*

A cost-effective, thin-film spin-coating method for homogeneous matrix deposition in matrix-assisted laser desorption/ionization mass spectrometry imaging (MALDI-MSI) is presented. In this method, the matrix solution is nebulized directly onto the sample surface during continuous rotation in the spin coater, enabling simultaneous spraying and centrifugal spreading for uniform film formation. Although spin coating produces highly uniform matrix layers, its widespread adoption in MALDI-MSI is hindered by the high cost of commercial instruments. To address this limitation, an in-house spin coater is developed and optimized. A fractional factorial design identified flow rate, matrix volume, and rotation speed as the most critical parameters for achieving uniform deposition. Under optimal conditions (60 psi, 10 μL·min^{-1}, 400 μL, and 10 cm at 35 a.u.), the system produces homogeneous matrix films across entire glass slides. The effectiveness of this integrated spray during spin method is demonstrated by imaging the distinct spatial distributions of key lipids and metabolites in mouse brain, strawberry, and carrot tissues. This work establishes the in-house spin coater as a feasible and robust tool for enhancing reproducibility and data quality in routine MALDI-MSI workflows.

1. Introduction

Mass spectrometry (MS) is an essential tool in a wide range of scientific areas, including biomedicine, food science, plant metabolomics, and environmental analysis.[1,2] Its high sensitivity and molecular specificity allow for the detailed characterization of complex samples, enabling the identification of metabolites, lipids, peptides, and other analytes of interest. While conventional MS methods based on direct infusion or chromatographic separation are well established, they typically lack spatial context, which is essential for studying heterogeneous systems and localized molecular processes.[1,3,4]

Mass spectrometry imaging (MSI) overcomes this limitation by providing spatially resolved molecular information, allowing analytes to be mapped directly on the surface of tissues, slides, food products, or plant materials.[5–7] Among MSI techniques, matrix-assisted laser desorption/ionization (MALDI) is widely employed to generate 2D ion density maps, providing valuable insights into the spatial distribution. In MALDI-MSI, the sample surface is coated with an organic matrix that assists in the desorption and ionization of analytes upon laser irradiation.[5,8,9] The quality, homogeneously, and thickness of the matrix layer are key factors influencing analytical performance.[10]

Matrix application methods, such as robotic spraying and sublimation, are commonly used in MALDI workflows, each offering benefits in terms of reproducibility or spatial fidelity.[11,12] However, these techniques may require high-cost instrumentation or present challenges related to analyte delocalization or matrix crystallization.[13] Spin-coating has emerged as a promising yet underutilized approach for matrix deposition. In our approach, the matrix solution is nebulized directly onto the sample surface during spin coater rotation, allowing centrifugal forces to spread the matrix uniformly in a single integrated step. This technique utilizes centrifugal force to produce homogeneous, thin films with high control over thickness and surface morphology, potentially enhancing the consistency and reproducibility of MALDI-MSI data.[13]

L. Í. L. Maciel, J. V. Roque, A. C. Batista Junior, G. H. M. Dufrayer, N. Balbino, A. R. Chaves, B. G. Vaz
Universidade Federal de Goiás
Chemistry Institute
Goiânia, Goiás 74690–900, Brazil
E-mail: jussara_roque@ufg.br
boniek@ufg.br

K. V. N. Cavalcante
Universidade Federal de Jataí
Institute of Health Science
Jataí, Goiás 75801–615, Brazil

M. D. Ferreira Junior
Universidade Federal de Campinas
Obesity and Comorbidities Research Center
Campinas, São Paulo 13083–864, Brazil

Supporting information for this article is available on the WWW under https://doi.org/10.1002/anse.202500117

Despite its potential, the use of spin coaters in MALDI-MSI remains limited, mainly due to the high cost of commercial systems.[14] As a solution, low-cost in-house spin coaters have been developed using repurposed components and open-source hardware. Nevertheless, the success of matrix deposition via spin-coating depends on multiple parameters, including spin speed, deposition volume, and solvent property, which require careful optimization to achieve optimal performance.[15,16] By integrating the spray application with continuous rotation, this method simplifies matrix deposition and reduces reliance on complex or expensive equipment. In this study, we propose the use of Design of Experiments (DoE) strategy to optimize matrix deposition using a low-cost, in-house-built spin coater. By systematically evaluating the influence of key deposition parameters, our goal is to establish a reproducible and accessible protocol for MALDI-MSI sample preparation. This integrated spray during spin approach was validated across different types of samples, including mouse brain tissues, fruits, and vegetables, highlighting its versatility and robustness under varying surface and morphological conditions.

2. Experimental Section

2.1. Chemicals and Reagents

Methanol HPLC-grade (>99.9%) was purchased from Tedia Company (Fairfield, USA). Ultrapurified water was obtained from MS2000 WFI equipment (Gehaka, São Paulo, Brazil). Optimal cutting temperature (OCT) compound, trifluoroacetic acid (≥99%) and 5-dihydroxybenzoic acid (DHB) were acquired from Sigma–Aldrich (Massachusetts, USA). Indium-tin-oxide (ITO)-coated glass slides were purchased from Bruker Daltonics (Bremen, Germany).

2.2. Construction and Operation of the in-House Spin Coater

The in-house spin coater used for matrix applications was constructed based on the design reported by Blaskievicz et al.[17] Their study demonstrated a homemade spin coater made with repurposed electronic components, proving to be a low-cost and efficient alternative for uniformly depositing thin films on surfaces. The device was capable of producing coatings with thickness variations of less than 5%, offering performance comparable to that of commercial equipment. Building on this design, the developed device employs a brushless direct current (BLDC) motor and the platter from a discarded hard disk drive (HDD) as the rotating platform for matrix deposition. The system is controlled by an Arduino Uno R3 microcontroller board, which manages a 32A electronic speed controller (ESC). The operational logic is based on reading an analog signal from a potentiometer, which serves as the user interface for speed adjustment. The analog value is mapped to a calibrated operational range between 70° and 85° using the Servo.h library, representing the minimum threshold required to initiate rotation and the maximum safe operating speed for the assembled system. This signal is then sent to the ESC to modulate the power supplied to the motor, thus controlling its rotational speed. To provide a more intuitive user interface, the same potentiometer value is converted to a 0–100 scale and displayed on an (OLED) organic light emitting diode screen, offering the operator visual feedback of the applied speed level. However, the system does not directly measure the actual rotational speed in revolutions per minute (RPM), instead relying on estimated values based on the pulse width modulation (PWM) signal, in which the duty cycle of the pulses controls the effective power delivered to the motor. Spin-coating enables precise control over spin parameters, allowing for reproducible and homogeneous matrix application suitable for MALDI-MSI sample preparation. The entire system was assembled using a mix of commercially available low-cost components and repurposed electronic waste, emphasizing both cost-effectiveness and sustainability. A detailed list of materials, including quantity, source (purchased or reused), and estimated cost, is provided in (Table S1, Supporting Information).

As illustrated in **Figure 1**, the in-house spin coater features a rotating platform equipped with an (LCD) liquid crystal display for speed monitoring and control, which is assembled primarily using repurposed electronic components. The setup also includes a syringe pump and a nebulizing gas system, which together enable the direct application of the matrix solution onto the sample slide. The matrix is nebulized continuously onto the sample while the slide rotates, allowing centrifugal force to spread the solution in real time and form a uniform layer. The syringe pump delivers the matrix solution at a controlled and reproducible flow rate, while the nebulizing gas facilitates the formation of fine microdroplets, enhancing uniform coverage of the sample surface. Figure 1 also summarizes the key parameters that influence matrix deposition via spin coating: A) gas pressure, B) solution flow rate, C) matrix volume, D) distance between the spray applicator and the substrate (height), and E) rotation speed. A thorough understanding of how these variables affect the deposition process is critical for achieving uniform matrix distribution, a prerequisite for high-quality MALDI-MSI data.

2.3. Sample and Matrix Preparation for MALDI-MSI

DHB was used as the MALDI matrix. A DHB solution (30 mg mL^{-1} in methanol: water, 70:30 v/v) containing 1% trifluoroacetic acid was uniformly applied to the tissue sections using an in-house spin coater. During the process, the matrix was nebulized onto the tissue surface while the sample was spinning, ensuring homogeneous spreading by centrifugal force. Brain tissues from mice, as well as carrot and strawberry samples, were fresh-frozen at −80 °C, embedded in OCT compound, and cryosectioned at −20 °C using a Leica CM3050 S cryostat (Leica Microsystems A/S, Germany) at a thickness of 15 μm for brain tissue, and 100 μm for carrot and strawberry. The resulting tissue slices were mounted on ITO-coated glass slides and stored at −80 °C until MALDI analysis. Prior to matrix application, the tissue sections

Research Article
doi.org/10.1002/anse.202500117
Chemistry Europe
European Chemical Societies Publishing

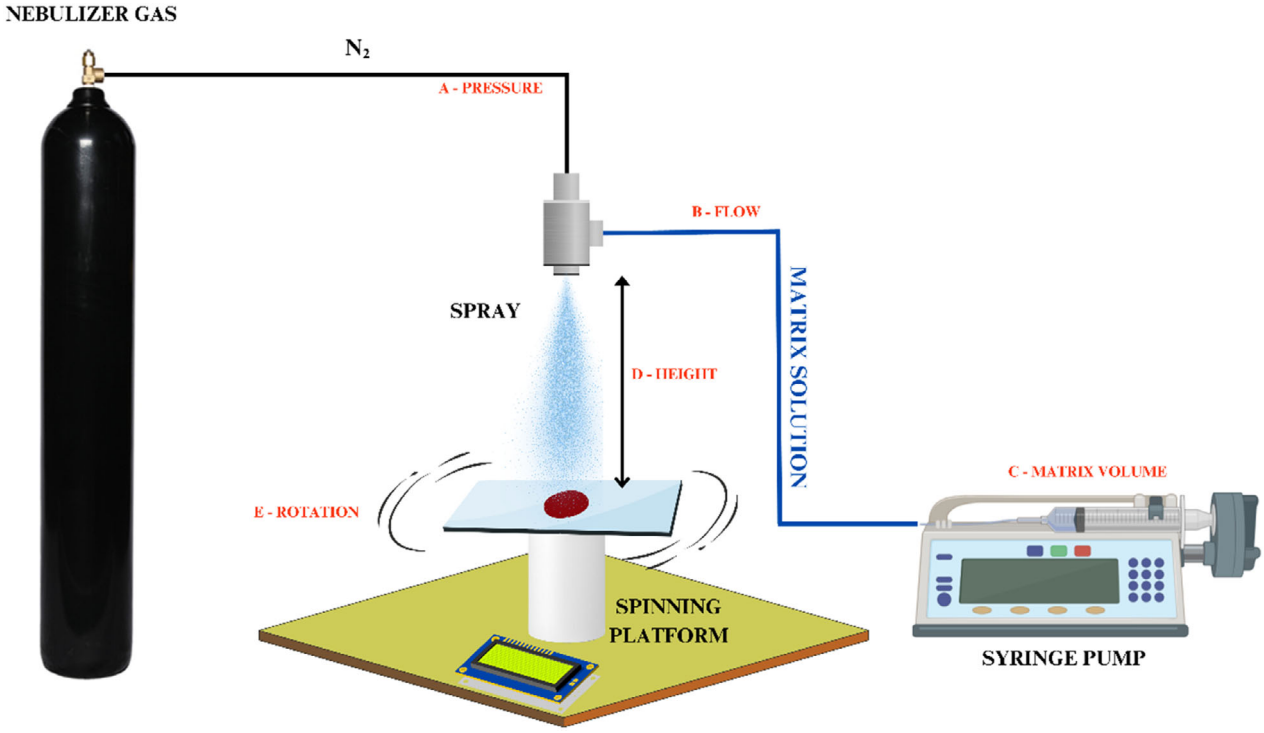

Figure 1. In-house spin-coater components and the main influential factors on spin-coating process.

were placed in a desiccator for 20 min to reduce residual moisture and improve matrix crystallization.

2.4. MALDI-FT-ICR MSI

MALDI-MSI analyses were performed using a 7 T solariX 2xR Fourier-transform ion cyclotron resonance mass spectrometer (FT-ICR-MS) (Bruker Daltonics, Bremen, Germany), equipped with a commercial MALDI ion source and a Nd:YAG laser operating at 355 nm. The instrumental parameters were set as follows: laser power at 65%, 250 laser shots per pixel, laser repetition rate of 1000 Hz, plate offset at −100 V, and the deflector plate to −220 V in negative ion mode. For positive ion mode: laser power at 60%, 220 laser shots per pixel, laser repetition rate of 1000 Hz, plate offset was set to 100 V, and the deflector plate to 220 V. A data reduction factor of 99% was applied. Spectra were acquired in magnitude mode with a transient size of 2 MW, using 2ω detection and a single scan across the *m/z* range of 140–1000. Matrix peaks of DHB at *m/z* 153.020 (negative ion mode) and *m/z* 273.045 (positive ion mode) were used as lock-masses to ensure mass accuracy within ±2 ppm. The mass resolving power was 100,000 at *m/z* 404.93123. MALDI images were acquired with a spatial resolution of 50 µm. Raw data were exported as *.imzML* and *.ibd* files using Scils Lab 2016a software (Bruker Daltonics, Bremen, Germany), and further processed in MATLAB 2024a (MathWorks, Natick, MA, EUA). Data processing, including binning (0.01 Da bin width), normalization to the total ion current (TIC), and Gaussian smoothing ($\sigma = 1.5$), were performed in-house using custom MATLAB scripts.

2.5. Matrix Application Optimization

Matrix deposition via spin-coating was optimized using a multivariate approach to determine the optimal process conditions with a reduced number of experiments. The experimental design aimed to ensure homogeneous matrix deposition onto the slide surface, using a simultaneous spray during spin approach. In this context, homogeneity refers to the uniform spatial distribution of matrix ions across the surface, which is essential to ensure reproducible ionization efficiency and signal consistency in MALDI-MSI. Inhomogeneous matrix layers can cause variations in ion signal intensity, negatively impacting the reliability of molecular imaging. Therefore, homogeneity is not only a desired physical property of the deposited layer but a key factor influencing the analytical quality of the imaging data.[18]

The selection of variables and their respective levels was guided by preliminary experiments employing the in-house spin coater, along with insights from a recent study by our research group (Bernardo et al.[19]). The chosen factors and their levels were chosen based on their demonstrated impact on the matrix deposition process. Hence, key parameters including nebulizing gas pressure, solvent flow rate and volume, distance between the applicator and the slide (height), and spin coater rotation speed, were evaluated using a 2^{5-2} fractional factorial design with a central point. Each variable was assessed at low, medium, and high levels, as detailed in **Table 1**. The design comprised eight experimental runs, along with a central point analyzed in quintuplicate.

Each chemical image, derived from the spatial distribution map of the matrix ion, was analyzed using macropixel analysis

Research Article
doi.org/10.1002/anse.202500117
Chemistry Europe
European Chemical Societies Publishing

Table 1. Experimental variables and their codified and decodified levels used in the fractional factorial design for matrix deposition optimization via spin-coating.

Variables	Codified levels		
	−1	0	+1
	Decodified levels		
Pressure [psi]	40	50	60
Flow [µL.min^{-1}]	10	15	20
Volume [µL]	200	300	400
Height [cm]	5	10	15
Rotation [au][a)]	35	45	55

[a)]**au: arbitrary unit**.

and the Poole homogeneity index. Macropixel analysis quantifies the heterogeneity of pixel clusters by dividing the image into nonoverlapping square macropixels and comparing their intensity variation.[20] This segmentation enables the calculation of the mean pixel intensity (X_M) and the standard deviation of pixel intensities (Sd), as described in Equations (1) and ((2)).

$$X_M = \frac{1}{p}\sum_{i=1}^{p} X_i \tag{1}$$

$$S_d = \sqrt{\frac{\sum_{i=1}^{p}(xi - X_M)^2}{p-1}} \tag{2}$$

Homogeneity, in this context, reflects the degree to which components are randomly distributed within the image. To estimate this parameter, the original image was compared to a randomized version containing the same pixel values but arranged without spatial order. From this comparison, the mean standard deviation of macropixels in the original image (M_{SDI}) and in the randomized image (M_{SDR}) was determined, as shown in Equation (3). These values were then used to calculate the Poole index, from which the Poole homogeneity ratio ($H\%_P$) was derived Equation (4).

$$M_{SD} = \frac{1}{mp}\sum_{i=1}^{mp} Sdi \tag{3}$$

$$H\%_p = \frac{M_{SDI}}{M_{SDR}} * 100 \tag{4}$$

Therefore, $H\%_P$ calculated values were used as response for the fractional factorial design 2^{5-2} as a measure of the homogeneity of the applied matrix. To determine the optimal deposition condition, a desirability function was applied aiming to maximize the $H\%_P$ value, with desirability increasing as the index approached 100, which represents a reference for ideal spatial homogeneity.[21] The influence of each factor was evaluated based on the normal probability plot of standardized effects, allowing the identification of statistically significant variables contributing to matrix deposition homogeneity. All image processing, calculations and statistical treatment were performed using custom-developed algorithms in MATLAB 2024a.

3. Results and Discussion

3.1. MALDI-FT-ICR MSI Analysis

To investigate the performance of matrix deposition under different conditions, specific *m/z* values related to DHB were selected for monitoring during MALDI-FT-ICR MSI analyses. Due to the acidic nature of DHB, an experimental design was primarily developed in the negative ion mode, where the molecule shows higher ionization efficiency.[22] Accordingly, *m/z* 153.020 and 307.031 were monitored in the negative ion mode, while *m/z* 273.045 and 313.032 were tracked in the positive ion mode, as illustrated in **Figure 2**. In all conditions tested, the matrix solution was applied using a simultaneous nebulization while spinning approach, in which the DHB solution was sprayed continuously during substrate rotation to ensure even distribution by centrifugal force.

The selection of *m/z* 153.020 in the negative ion mode corresponds to the deprotonated DHB molecule $[DHB–H]^-$, consistent with its ability to form negative ions.[23] The ion at *m/z* 307.031 likely represents a deprotonated DHB dimer $[2DHB–H]^-$ (Figure 2A), which is commonly observed under conditions of dense matrix crystallization or in the presence of specific solvent effects.[24] Although DHB possesses acidic hydroxyl and carboxylic groups that facilitate deprotonation and favor ion generation in the negative mode, it is predominantly used as a MALDI matrix in the positive ion mode. This preference is attributed to the nature of the MALDI desorption/ionization plume, where abundant reactive species such as $[M + H]^+$, $[M + Na]^+$, and $[M + K]^+$ are generated through proton and cation transfer from the matrix to the analyte via collisions that occur within the rapidly expanding plume initiated by ultraviolet laser irradiation.[22,25] DHB also forms matrix clusters that can coionize with analytes, further promoting the formation of diverse adducts, such as protonated dimers and trimers, and enhancing ionization efficiency in positive ion mode.[22] Therefore, we included *m/z* 273.045 $[2DHB-2H_2O + H]^+$ and 313.032 $[2DHB\text{-}H_2O + Na]^+$ in positive mode as representative signals of DHB and its clusters or adducts (Figure 2B).[26] The inclusion of these values aimed to demonstrate the efficiency of matrix distribution in both ionization conditions, corroborating the robustness and versatility of the matrix coating method developed in this study.

3.2. Multivariate Optimization to Matrix Deposition via Spin-Coating

Spin-coating is a highly recommended method for the deposition of thin films and substrates in applications requiring rapid and homogeneous coverage. This efficiency arises from the combination of centrifugal force and the surface tension of the applied substrate, which, under high-speed rotation, enables uniform coating over the entire surface.[27] Such characteristics are particularly

Research Article
doi.org/10.1002/anse.202500117
Chemistry Europe
European Chemical Societies Publishing

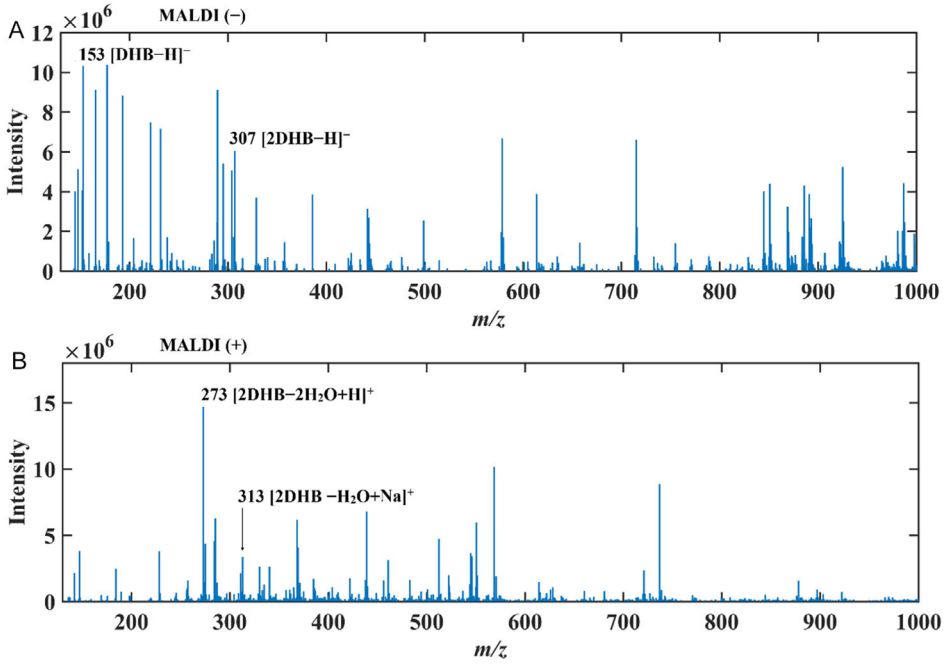

Figure 2. Mass spectra of DHB acquired in both A) negative and B) positive ion modes by MALDI-FT-ICR MSI. In negative mode, the ions at *m/z* 153.020 ($[DHB–H]^-$) and 307.031 ($[2DHB–H]^-$) were monitored, while in positive mode, *m/z* 273.045 $[2DHB + \cdot 2H_2O+H]^+$ and 313.032 $[2DHB+H_2O+Na]^+$ were selected. These ions were used as markers to evaluate the efficiency and reproducibility of matrix deposition under different experimental conditions.

advantageous for matrix deposition in chemical imaging by MALDI FT-ICR MSI. In this technique, it is essential that the matrix coating is spatially uniform across the entire sample, as ionization of the analytes relies heavily on the matrix. A homogeneous matrix layer ensures that all analytes are ionized in a similar manner, resulting in more accurate spatial representations of the molecular distribution within the sample, which is an aspect of critical importance in chemical imaging protocol. In our setup, the spin-coating process involves real-time nebulization of the matrix solution onto the sample while it is rotating, allowing centrifugal force to promote uniform distribution immediately upon deposition.

In the context of matrix deposition for MALDI-FT-ICR MSI, an in-house spin coater was constructed using electronic waste, following the approach described by Blaskievicz and colleagues.[17] This low-cost device was integrated into our setup and enabled continuous nebulization of the DHB matrix during sample rotation. Preliminary experiments revealed a marked dependence of ionization efficiency on key spin-coating parameters, reinforcing the need for systematic optimization to ensure homogeneous matrix application and reliable spatial molecular imaging.

Before implementing the multivariate optimization, preliminary experiments were conducted using the nebulization system without sample rotation. These initial trials revealed poor reproducibility and highly uneven matrix coverage, especially at the edges of the sample surface, likely due to the absence of centrifugal force to assist in matrix spreading. These limitations compromised matrix homogeneity and ion signal consistency. Therefore, a rotating platform was introduced to enhance distribution uniformity during nebulization, forming the basis for the integrated spin and spray approach adopted in this study.

To investigate the influence of the main spin-coating parameters on matrix deposition homogeneity for MALDI-FT-ICR MSI, a multivariate optimization was carried out using a fractional factorial design 2^{5-2}, evaluating five factors in two levels. This approach allows the assessment of both individual and interaction effects among the variables while reducing the number of experimental runs. **Table 2** and **Figure 3** present the 13

Table 2. Experimental conditions from the 2^{5-2} fractional factorial design and the corresponding calculated homogeneity indices ($H\%_P$) for matrix deposition, based on MALDI-FT-ICR MSI images in negative ion mode.

Experiments	Pressure [psi]	**Flow [µL.min^{-1}]**	Volume [µL]	Height [cm]	Rotation [au][a)]	**H $\%_P$**
1	40	10	200	15	55	83
2	60	10	200	5	35	99
3	40	20	200	5	55	70
4	60	20	200	15	35	84
5	40	10	400	15	35	99
6	60	10	400	5	55	86
7	40	20	400	5	35	81
8	60	20	400	15	55	71
9	50	15	300	10	45	85
10	50	15	300	10	45	85
11	50	15	300	10	45	84
12	50	15	300	10	45	85
13	50	15	300	10	45	85

[a)]**au: arbitrary unit**.

Research Article
doi.org/10.1002/anse.202500117
Chemistry Europe
European Chemical Societies Publishing

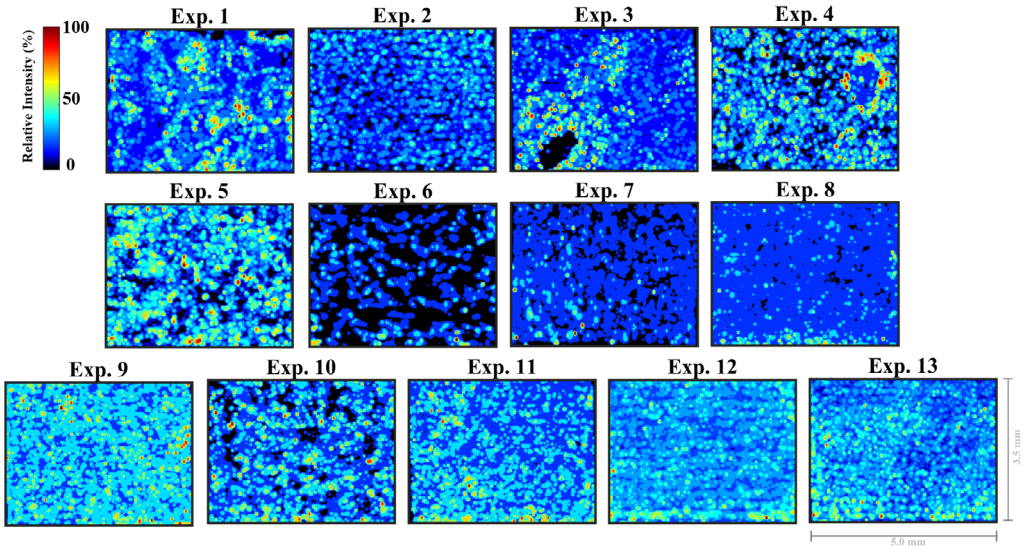

Figure 3. MALDI ion images of the DHB matrix ion at *m/z* 153.020 acquired in negative ion mode, obtained from each experimental condition tested in the fractional factorial design. All images were normalized to relative intensity and displayed on a consistent 0%–100% scale.

experiments, which were conducted in a random order. In each experiment, DHB was selected as the MALDI-FT-ICR MSI matrix, and its spatial distribution (*m/z* 153.020) was used as a parameter to evaluate the homogeneity of matrix application via the spin-coating process. Accordingly, the DoE experiments were conducted on ITO-coated slides without samples, onto which thin layers of the DHB matrix were deposited by continuous nebulization during spinning. The ion image corresponding to *m/z* 153.020 was used as a parameter for homogeneity assessment. Homogeneity was accessed using Poole homogeneity ratio ($H\%_P$), and these indices were used as response for the performed a fractional factorial design.

Figure 3 presents the spatial distribution of the DHB matrix (*m/z* 153.020), which was applied by nebulization simultaneously with substrate rotation using the spin-coating device, for the 13 experiments conducted within the fractional factorial design. These ion images clearly demonstrate that the selected factors influence the homogeneity of matrix deposition. Based on these spatial distributions, $H\%_P$ were calculated by comparing the original images to their randomized counterparts, which retain identical pixel intensity values within a different spatial organization. For this purpose, each ion image was segmented into ten macropixels (10×7 array) of size 10×10 pixels. The $H\%_P$ index was subsequently used as the response (dependent variable) in the experimental design, enabling the assessment of how each factor at low, medium, and high levels affects matrix deposition homogeneity.

Initially, the standardized effects of each factor on matrix homogeneity were evaluated through a normal probability plot, enabling the identification of the most influential factors in the in-house spin-coating process. This type of plot is a fundamental tool in DoE approaches, as it enables the visual identification of the most influential factors on a given response by distinguishing statistically significant effects from random variations. **Figure 4** demonstrates the normal probability plot of the factors evaluated in the fractional factorial design. By evaluating the magnitude of t-value and the deviation of the expected normal values, it is evident the influence of the flow rate and rotation speed on the matrix homogeneity on a spin coater process. Both factors exhibited negative standardized effects, indicating that increasing either parameter led to a decrease in the homogeneity of matrix deposition. In contrast, gas pressure, matrix volume, and height of the spray nozzle despite being part of the integrated nebulization rotation process demonstrated minimal effects on the matrix homogeneity.

To better understand the influence of each factor within the studied range, the desirability function was applied. This approach, commonly employed in DoE, aims to identify the optimal levels of individual factors that either maximize or minimize the response of interest. The desirability function is scaled from 0 to 1, with values closer to 1 indicating conditions that are more

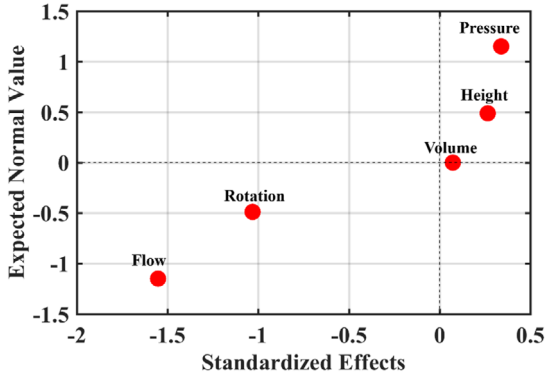

Figure 4. Normal probability plot of standardized effects from the 2^{5-2} fractional factorial design, illustrating the influence of each deposition parameter on matrix homogeneity ($H\%_P$) in MALDI-FT-ICR MSI.

Research Article
doi.org/10.1002/anse.202500117
Chemistry Europe
European Chemical Societies Publishing

favorable or aligned with the target process outcome. In the context of matrix deposition via spin coating, the desirability function was constructed to maximize matrix homogeneity while maintaining operational feasibility.

Therefore, the fractional factorial design allowed the assessment of the desirability profile of each factor in the studied levels, observed in **Figure 5**. The desirability plot provided a simultaneous visualization of the predicted response behavior and the corresponding desirability function. The dashed red line in each desirability plot represents the optimal level of the corresponding factor, as determined by the global desirability function. This position indicates the specific setting that, in combination with the other factors, contributes to maximizing the overall desirability of the process outcome. Once more, it became clear that flow rate and rotation were the most influential parameters on the spin coating process.

Alongside, the desirability function provided the surface contour plots, which are a valuable tool to understand the experimental space in two dimensions. These plots combine two factors and illustrate how the experimental space responds to their simultaneous variation, thereby facilitating the identification of potential synergistic effects between them and supporting informed decision-making. The color scale used in the contour plots represents the magnitude of the desirability function, ranging from 0 (least desirable) to 1 (most desirable). This gradient provides an intuitive visual cue for identifying regions of higher or lower desirability within the experimental space. In this study, contour surface plots (**Figure 6**) were analyzed to identify the optimal region within the experimental space, represented by the warmer areas. These findings are consistent with the previously observed desirability profiles, confirming that the highest desirability was achieved when both flow rate and rotation speed were set at their lower levels, while the matrix volume was at its highest. Additionally, the plots reinforced that height and gas pressure had minimal influence on the matrix deposition process. The overall flatness of the contour surfaces further indicates the absence of synergistic interactions between the evaluated factors.

Overall, increasing the matrix flow rate negatively impacted the uniformity of matrix deposition on the sample surface, likely due to difficulties in forming a stable spray. Experimentally, a flow rate of 20 $\mu L.min^{-1}$ led to droplet formation in the spray, even under tested nebulizing gas pressure was applied. It is important to note that the pressure range investigated was sufficient to ensure matrix delivery onto the slide. Additionally, the effect of matrix volume on deposition homogeneity can be attributed to the thickness of the applied matrix layer. Lower flow rates promoted more controlled deposition of thinner layers, promoting the formation of small, homogeneous crystals. In contrast, higher flow rates tend to cause oversaturation of the surface, resulting in the formation of larger, irregular crystals that compromise both the homogeneity of the matrix and the ionization efficiency of analytes.

Similarly, rotation speed significantly influenced matrix homogeneity. In the spin coating setup, the sample slide was mounted on a rotating platform and different rotation speeds were applied. The fractional factorial design revealed that lower rotation speeds favored more homogeneous matrix distribution. This effect can be attributed to the influence of rotation on solvent evaporation dynamics. At higher rotation speeds, rapid evaporation of the matrix solvent likely occurs, leading to the formation of irregular and heterogeneous crystals. In contrast, slower speeds allow for more gradual evaporation, providing a controlled environment for nucleation and crystal growth. Additionally, centrifugal force may contribute to the observed effects. As rotation speed increases, the centrifugal force may drive the matrix solution outward, causing uneven distribution from the center toward the edges of the slide. This centrifugal dispersion was visually evident at the end of the deposition process. Therefore, lower rotation speeds promote more homogeneous matrix deposition by enabling uniform crystal formation and minimizing dispersive effects.

The fractional factorial design also revealed the positive effect of increasing the volume of matrix solution applied. Notably, higher volumes led to greater deposition homogeneity, which can be attributed to the increased amount of DHB mass delivered

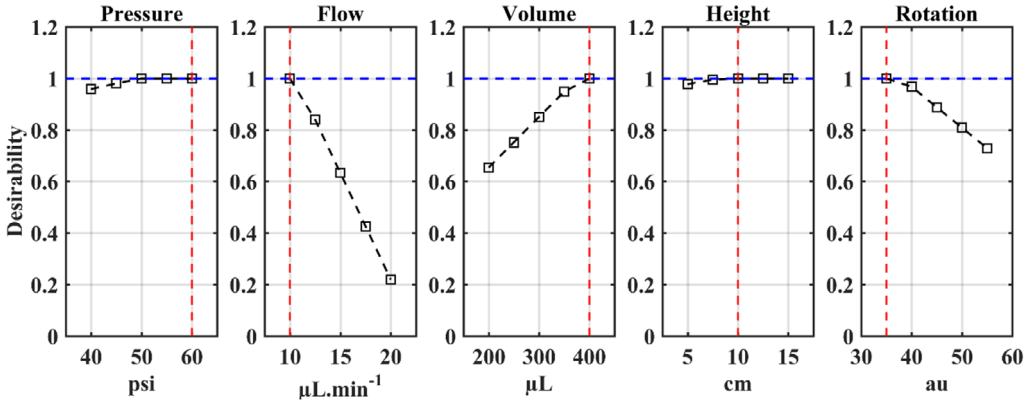

Figure 5. Desirability plots for each variable in the fractional factorial design, showing the influence of deposition parameters on the homogeneity index ($H\%_P$) in MALDI-FT-ICR MSI. The blue dashed line represents the maximum desirability (1.0), while the red dashed line indicates the optimal value for each parameter.

Research Article
doi.org/10.1002/anse.202500117
Chemistry Europe
European Chemical Societies Publishing

onto the slide, ensuring complete and uniform matrix coverage. Furthermore, the design demonstrated that the height of the spray source and the nebulizing gas pressure had minimal influence on matrix deposition using the spin-coating approach, suggesting that variations in these parameters were not significant for the homogeneity of the deposited layer.

The fractional factorial design led to the optimal condition for matrix deposition homogeneity in MALDI-FT-ICR MSI analyses. This optimal condition was achieved under the following conditions: gas pressure of 60 psi; application flow rate of 10 µL.min^{-1}; applied volume of 400 µL; height of 10 cm; and rotation speed of 35 au. The optimal point was evaluated in quintuplicate (**Figure 7**), assessing matrix deposition homogeneity in both negative ion mode (*m/z* 153.020 and *m/z* 307.031) and positive ion mode (*m/z* 273.045 and *m/z* 313.032). These experiments demonstrated high matrix homogeneity, with H%$_P$ values reaching up to 99%.

3.3. Optimized MALDI FT-ICR MSI Protocol on Biological and Plant Tissue Slices

The optimized matrix deposition condition was applied to the analysis of several real samples, including mouse brain tissue, carrot, and strawberry. Mouse brain tissue sections were analyzed by MALDI-FT-ICR MSI in negative and positive ion mode, yielding chemical images with excellent spatial resolution (**Figure 8**). It is important to note that the slight angulation observed in some tissue sections, such as those shown in Figure 8, results from the mounting procedure of the tissue slices on the ITO slides and is unrelated to the matrix application method. During the spin-coating process, the tissue sections remain securely fixed to the slide surface, and the rotational speeds employed are carefully controlled to avoid mechanical stress or damage. Therefore, the spin and spray method does not alter tissue morphology or compromise sample integrity prior to MALDI-MSI analysis. Among the detected ions, prominent signals at *m/z* 862.609 (error: 0.98 ppm; intensity: 9.2×10^5) and *m/z* 878.594 (error: 1.01 ppm; intensity: 4.7×10^6) were observed, corresponding to the sulfated sphingolipids SHexCer 40:1;O2 and SHexCer 40:1;O3 (see the mass spectra in Figure S1A, Supporting Information). These lipids exhibited predominant distribution in the corpus callosum, a region rich in myelinated fibers, consistent with the structural role of SHexCer in maintaining the myelin sheath. Furthermore, these species have been associated with neuroinflammatory and demyelinating processes in neurodegeneration models. These ions have been previously mapped in MALDI-FT-ICR MSI studies of brain tissue, demonstrating characteristic localization in myelinated regions such as the corpus callosum.[28–30]

In positive ion mode, were observed *m/z* 810.601 attributed to phosphatidylcholine PC (38:4) $[M + K]^+$ (error 0.95 ppm; intensity: 6.8×10^5), and *m/z* 828.523, corresponding to

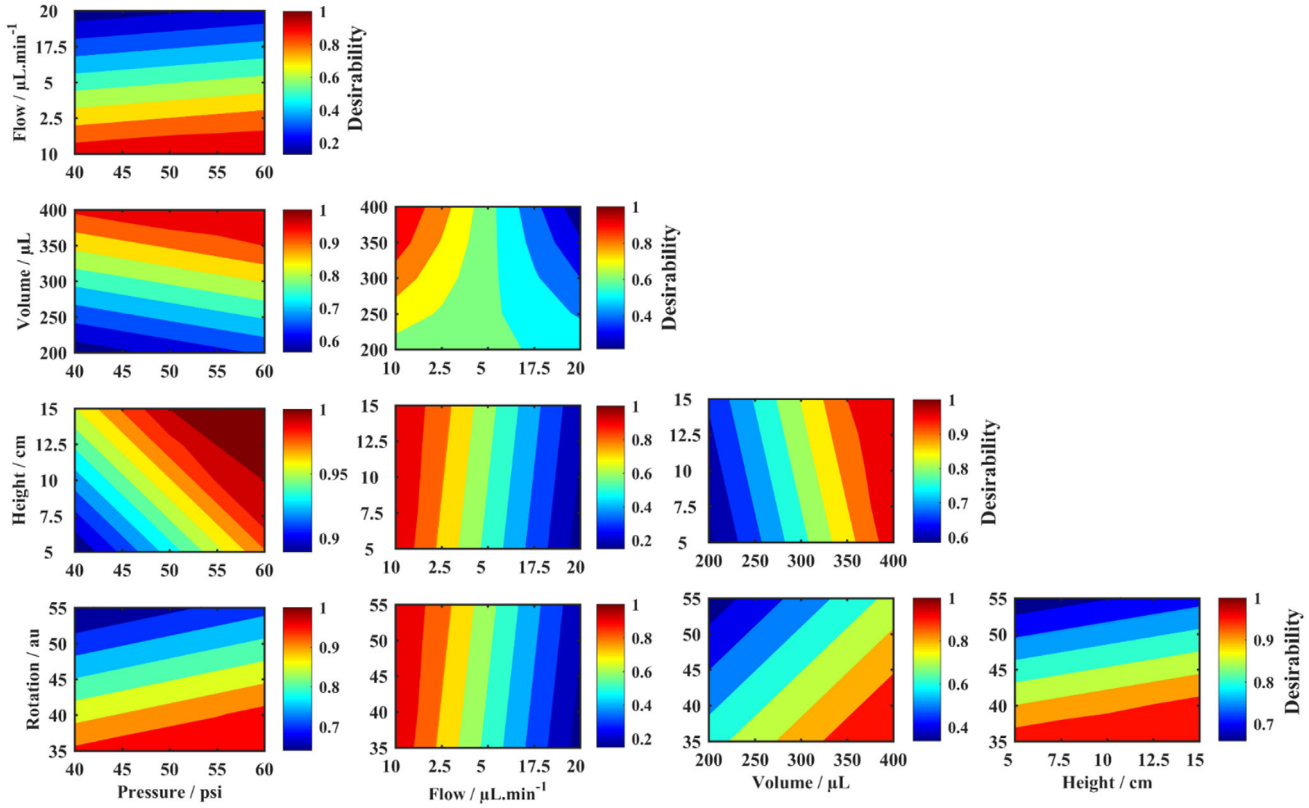

Figure 6. Desirability surface contours plots for pairwise combinations of deposition parameters evaluated in the 2^{5-2} fractional factorial design. The plots illustrate the effect of each variable interaction on the predicted desirability, which was calculated to maximize the homogeneity index (H%$_P$) in MALDI-FT-ICR MSI experiments. Warmer colors indicate regions of higher desirability.

Research Article
doi.org/10.1002/anse.202500117
Chemistry Europe
European Chemical Societies Publishing

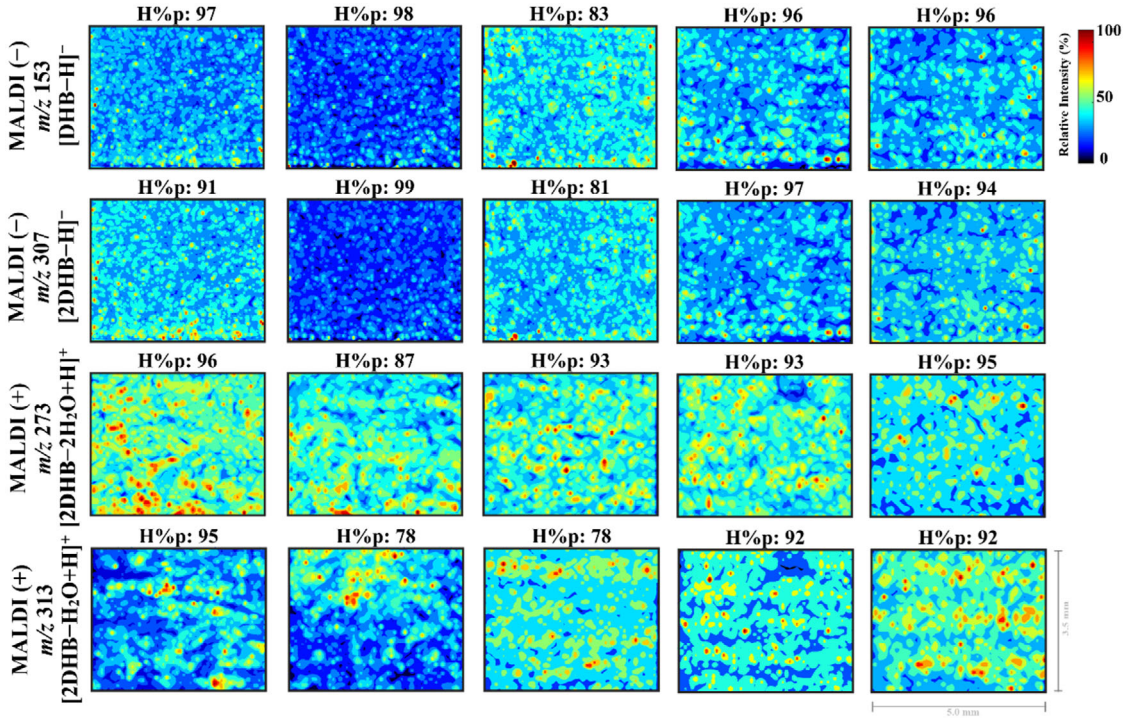

Figure 7. MALDI-FT-ICR MSI ion images of four selected matrix-related ions acquired from five replicates under the optimized deposition condition established by the fractional factorial design. The images include two ions acquired in negative ion mode (*m/z* 153.020 and *m/z* 307.031) and two in positive ion mode (*m/z* 273.045 and *m/z* 313.032). All images were normalized to relative intensity and evaluated for spatial uniformity using the Poole homogeneity index ($H\%_P$).

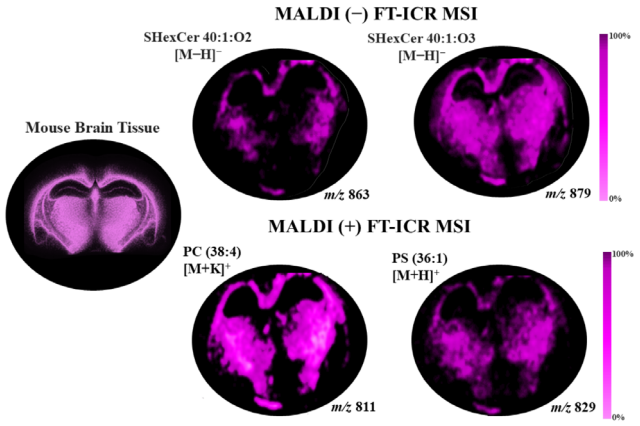

Figure 8. Ion images obtained by MALDI FT-ICR MSI in both negative and positive ion modes from mouse brain tissue sections, acquired using the optimized matrix deposition protocol via spin coating. The ions at *m/z* 862.609 and *m/z* 878.594, corresponding to the sulfated sphingolipids SHexCer 40:1;O2 and SHexCer 40:1;O3, respectively, exhibit predominant localization in the corpus callosum. In the positive ion mode, the ions at *m/z* 810.601 attributed to PC (38:4) $[M-K]^+$ and *m/z* 828.523 corresponding to PS (36:1) $[M+H]^+$,show distinct spatial distributions across the brain. A schematic representation of the mouse brain is included to highlight the corpus callosum region and aid anatomical orientation.

phosphatidylserine PS (36:1) $[M+H]^+$ (error 0.97 ppm; intensity: 3.6×10^5) (Figure S1B, Supporting Information). Both lipid species were predominantly localized within the corpus callosum, although with distinct relative intensities. This colocalization suggests a region-specific accumulation of these phospholipids, which may be associated with the structural and functional specificity of the corpus callosum, a white matter region rich in myelinated axons. The higher signal intensity of PC (38:4) may reflect its abundance in myelin sheaths or its role in maintaining membrane integrity and signaling within oligodendrocytes. In contrast, the lower abundance of PS (36:1), despite being codetected in the same region, may indicate its more specific involvement in cell signaling or apoptotic processes. These findings highlight the capability of MSI to discriminate subtle variations in lipid composition within anatomically defined brain regions. Consistent with our results, previous MALDI-MSI investigations have demonstrated the regional distribution of PC (38:4) and PS (36:1) within the corpus callosum, highlighting their enrichment in myelin-rich structures and their potential roles in membrane architecture and cell signaling in the central nervous system.[31–33]

In addition to brain tissue, the optimized matrix deposition protocol was successfully applied to plant-based samples. MALDI FT-ICR MS analysis of a carrot slice, acquired in negative and positive ion mode, enabled the detection of key metabolic constituents with high spatial resolution and mass accuracy (**Figure 9**). In the negative ion mode, two prominent ions were detected: *m/z* 145.060 attributed to Glutamine $[M-H]^-$ (error 0.97 ppm; intensity: 1.6×10^6), and *m/z* 353.085, corresponding to Chlorogenic acid $[M-H]^-$ (error 0.76 ppm; intensity: 8.3×10^6) (Figure S2A, Supporting Information). Glutamine, a central amino acid in nitrogen assimilation and amino acid biosynthesis, showed widespread distribution with higher intensity in

Research Article
doi.org/10.1002/anse.202500117
Chemistry Europe
European Chemical Societies Publishing

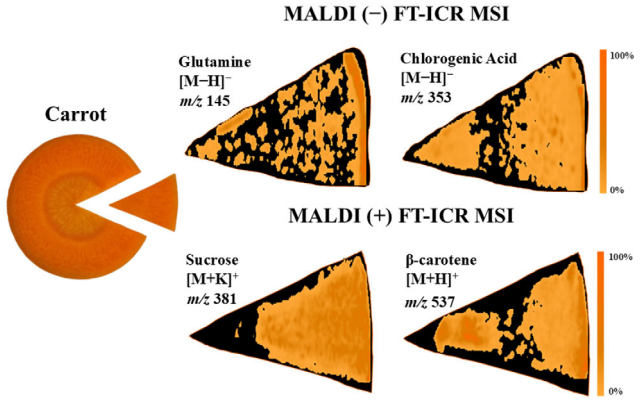

Figure 9. Ion images obtained by MALDI-FT-ICR MSI in both negative and positive ion modes from carrot tissue sections, acquired using MALDI FT-ICR MS. In the negative ion mode, *m/z* 145.060 and *m/z* 353.085 correspond to Glutamine ($[M-H]^-$) and Chlorogenic Acid ($[M-H]^-$), respectively. In the positive ion mode, the ions at *m/z* 381.079 and *m/z* 537.445 correspond to sucrose ($[M+K]^+$) and β-carotene ($[M+H]^+$), respectively. These ion images reveal the spatial distribution of metabolites across the carrot section, highlighting differential localization patterns. A schematic representation of the carrot cross-section is included for reference.

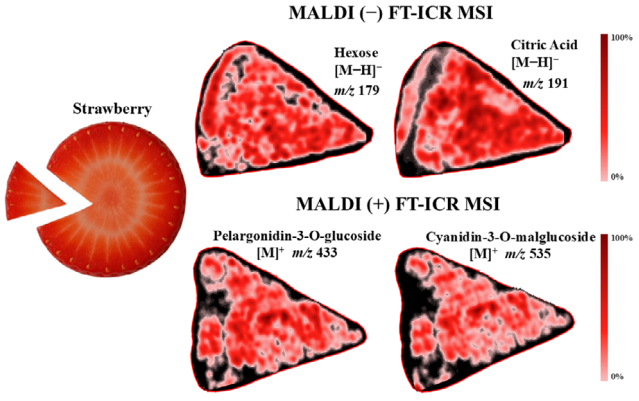

Figure 10. Ion images obtained by MALDI-FT-ICR MSI in both negative and positive ion modes from strawberry tissue sections. In the negative ion mode, *m/z* 179.055 and *m/z* 191.018 correspond to Hexose ($[M-H]^-$) and Citric Acid ($[M-H]^-$), respectively, showing distinct spatial distributions throughout the fruit section. In the positive ion mode, two anthocyanins were identified: *m/z* 433.113, corresponding to pelargonidin-3-O-glucoside $[M]^+$, and *m/z* 535.108 attributed to cyanidin-3-O-malglucoside $[M]^+$. A schematic representation of the strawberry cross-section is shown to support interpretation.

the outer cortex, suggesting active metabolic and defense processes in peripheral parts.[34,35] Chlorogenic acid, a phenolic antioxidant involved in plant defense and stress regulation, was predominantly localized in the core and inner pulp, with low intensity in the transition zone, indicating spatial control of phenolic accumulation.[36] Notably, these same ions were also identified in a previous by liquid chromatography coupled to MS (LC-MS) analysis of carrot biomass, supporting their relevance as characteristic metabolites of this matrix.[37]

In the positive ion mode, we observed *m/z* 381.079, attributed to sucrose $[M+K]^+$ (error 0.79 ppm; intensity: 3.9×10^7), and *m/z* 537.445, corresponding to β-carotene $[M+H]^+$ (error 0.94 ppm; intensity: 8.3×10^6), (see the mass spectra in Figure S2B, Supporting Information). Sucrose, a key transport sugar and energy source, was abundant throughout the slice, except for a marked reduction in the central pith, possibly reflecting lower metabolic activity in this region.[38] In contrast, β-carotene, a precursor of vitamin A and a major antioxidant pigment, showed high intensity across most of the tissue, with decreased levels at the pulp–core boundary, suggesting localized regulation of carotenoid accumulation.[39] These findings are consistent with previous MALDI-MSI studies that successfully detected β-carotene in carrot and disaccharides such as sucrose in apple and processed food samples like veal sausage, demonstrating the capability of this technique to resolve a broad spectrum of metabolites, ranging from highly nonpolar pigments to polar sugars, across various food matrices.[40–42]

MALDI FT-ICR MSI analysis was also applied to strawberry slices, which is a fruit widely consumed for its appealing flavor and rich nutritional profile, including sugars, organic acids, flavonoids, and vitamins.[43,44] Analyses in both negative and positive ion modes enabled spatial mapping of key metabolites within the slice (**Figure 10**). In the negative ion mode, two main compounds were identified: *m/z* 179.055 attributed to Hexose $[M-H]^-$ (error 0.54 ppm; intensity: 9.7×10^5) and *m/z* 191.018 correspond to Citric Acid $[M-H]^-$ (error 0.20 ppm; intensity: 7.4×10^7) (Figure S3A, Supporting Information). The presence of sugars (such as fructose, glucose, and sucrose) in strawberries is well documented in the literature, as these molecules play a role in defining the fruit's sweet flavor.[45,46] Hexoses are central to metabolic pathways and contribute to the biosynthesis of phenolic compounds. In our study, hexose exhibited strong and widespread signal intensity across the tissue, supporting its physiological significance. Citric acid, the predominant organic acid in strawberries, was also detected with high abundance and uniform spatial distribution. As a key metabolite in the tricarboxylic acid cycle, it plays an important role during ripening. Citric acid (*m/z* 191.018) was detected with high abundance and uniform spatial distribution. This finding aligns with prior metabolomic reports and reinforces its value as both a biochemical and sensory marker in strawberry slice.[46,47]

In positive ion mode, two anthocyanins were identified: *m/z* 433.113, corresponding to pelargonidin-3-O-glucoside $[M]^+$ (error 0.23 ppm; intensity 2.9×10^6), and *m/z* 535.108 attributed to cyanidin-3-O-malglucoside $[M]^+$ (error 0.47 ppm; intensity 1.1×10^6) (Figure S3B, Supporting Information).[45,48,49] These compounds are directly associated with the characteristic red-to-pink pigmentation of strawberries and represent key metabolites involved in the visual and nutritional attributes of the fruit.[49] As shown in Figure 10, both pigments exhibited similar spatial distribution patterns, with higher signal intensities detected in the inner regions of the tissue, gradually decreasing toward the outer skin. This spatial distribution aligns with previous finds that indicate the accumulate of anthocyanins in the pulp and internal layers during specific ripening stages of the fruit.[44,45]

Both the analysis of mouse brain tissue and the evaluation of plant slices from carrot and strawberry demonstrated the high efficiency of the spin-coating protocol, which integrates

controlled nebulization during rotation for matrix deposition in promoting the ionization of endogenous compounds. The optimized spin-coating approach provided accurate and reproducible spatial localization of the analytes, enabling reliable inferences regarding their distribution within the samples. These results agree with previous MALDI-MSI studies reported in the literature, further validating our findings.

Notably, recent comparative studies using commercial matrix application systems, such as the HTX M3+ sprayer and sublimation techniques, have reported similar outcomes regarding analyte localization and image homogeneity.[15,50–52] In the present work, a direct quantitative comparison with commercial systems was not performed, as our main objective was to demonstrate the feasibility and reproducibility of the in-house spin coater. Nevertheless, our qualitative results support the effectiveness of the in-house spin coater as a cost-efficient alternative, capable of producing MALDI-MSI data of comparable quality for various sample types. Collectively, these outcomes highlight the potential of this method to expand the frontiers of chemical imaging by MALDI-MSI.

4. Conclusion

The results of this study highlight the effectiveness of a custom-built- spin-coating based system, which integrates controlled matrix nebulization during rotation, for achieving homogeneous matrix deposition in MALDI-MSI experiments. This strategy provided a robust and reproducible means of applying the DHB matrix as a thin film, which is essential for ensuring high spatial fidelity in chemical imaging. By evaluating matrix distribution uniformity using the $H\%_P$ metric, we demonstrated that our optimized conditions consistently produced films with near-ideal homogeneity.

The approach proved to be versatile and adaptable to different sample types, including both biological (mouse brain) and plant (strawberry and carrot) tissues, supporting high-quality spatial ion distribution maps. Notably, the optimized matrix deposition procedure facilitated the ionization and visualization of relevant endogenous compounds, including lipids, sugars, and small organic acids, thereby confirming its broad applicability across various sample classes.

Beyond the specific results presented, this work contributes to the field by offering an accessible and low-cost alternative to commercial deposition systems, with potential to democratize high-performance MALDI-MSI analysis in laboratories with limited resources. The combined use of systematic optimization and spatial uniformity metrics establishes a solid foundation for further development of hybrid matrix application techniques in MSI.

Acknowledgements

This study was financed in part by the Coordenação de Aperfeiçoamento de Pessoal de Nível Superior - Brasil (CAPES) - Finance Code 001. The authors were grateful to Fundação de Amparo à Pesquisa do Estado de Goiás (FAPEG) (grant nos. 20180267001519, 202310267001395, and 202110267000436) and Conselho Nacional de Desenvolvimento Científico e Tecnológico (CNPq).

The Article Processing Charge for the publication of this research was funded by the Coordenação de Aperfeiçoamento de Pessoal de Nível Superior - Brasil (CAPES) (ROR identifier: 00x0ma614).

Conflict of Interest

The authors declare no conflict of interest.

Data Availability Statement

The data that support the findings of this study are available from the corresponding author upon reasonable request.

Keywords: 5-dihydroxybenzoic acid · Fourier-transform ion cyclotron resonance mass spectrometer · mass spectrometry imaging · multivariate optimization · spin-coating

[1] X. Zhang, Q. Li, Z. Xu, J. Dou, *RSC Adv.* **2020**, *10*, 3092.
[2] T. F. Jorge, A. T. Mata, C. António, *Philos. Trans. R. Soc. A* **2016**, *374*, 20150370.
[3] N. K. Anh, N. Q. Thu, N. T. N. Tien, N. P. Long, H. T. Nguyen, *Molecules* **2024**, *29*, 5934.
[4] X. Min, Y. Zhao, M. Yu, W. Zhang, X. Jiang, K. Guo, X. Wang, J. Huang, T. Li, L. Sun, J. He, *Clin. Transl. Med.* **2024**, *14*, e70031.
[5] H. Liu, Y. Pan, C. Xiong, J. Han, X. Wang, J. Chen, Z. Nie, *TrAC Trends Anal. Chem.* **2022**, *157*, 116809.
[6] P. Bourceau, B. Geier, V. Suerdieck, T. Bien, J. Soltwisch, K. Dreisewerd, M. Liebeke, *Nat. Protoc.* **2023**, *18*, 3050.
[7] L.-X. Nie, J. Dong, L.-Y. Huang, X.-Y. Qian, C.-J. Lian, S. Kang, Z. Dai, S.-C. Ma, *Front. Pharmacol.* **2021**, *12*, 685575.
[8] X. Zhu, T. Xu, C. Peng, S. Wu, *Front. Chem.* **2022**, *9*, 782432.
[9] A. A. Patil, M. J. N. Descanzo, V. B. Dhisale, W.-P. Peng, *Int. J. Mass Spectrom.* **2024**, *498*, 117219.
[10] C. Meisenbichler, C. Doppler, D. Bernhard, T. Müller, *Anal. Bioanal. Chem.* **2019**, *411*, 3221.
[11] L. Í .L. Maciel, R. A. Bernardo, R. O. Martins, A. C. B. Junior, J. V. A. Oliveira, A. R. Chaves, B. G. Vaz, *Anal. Bioanal. Chem.* **2023**, *415*, 4125.
[12] K. Susniak, M. Krysa, B. Gieroba, I. Komaniecka, A. Sroka-Bartnicka, *Acta Biochim. Pol.* **2020**, *67*, 277.
[13] L. R. S. Huizing, S. R. Ellis, B. W. A. M. M. Beulen, F. P. Y. Barré, P. B. Kwant, R. J. Vreeken, R. M. A. Heeren, *Clin. Mass Spectrom.* **2019**, *12*, 7.
[14] D. C. Rubio, W. Weber, E. Klotzsch, *HardwareX.* **2022**, *11*, e00316.
[15] C. Tressler, S. Tilley, E. Yang, C. Donohue, E. Barton, A. Creissen, K. Glunde, *J. Am. Soc. Mass Spectrom.* **2021**, *32*, 2728.
[16] A. Chepluki, T. Frizon, I. de Carvalho, *Quim. Nova* **2023**, *46*, 470.
[17] S. Blaskievicz, L. Soares, L. Mascaro, *Quim. Nova* **2021**, *44*, 1180.
[18] M. Kompauer, S. Heiles, B. Spengler, *Nat. Methods* **2017**, *14*, 90.
[19] R. A. Bernardo, C. I. de Oliveira Júnior, J. V. Roque, N. do L. Costa, V. M. Roriz, C. A. Sorgi, C. Janfelt, B. G. Vaz, A. R. Chaves, *J. Proteome Res.* **2024**, *23*, 2750.
[20] L. R. Terra, J. V. Roque, C. C. Pola, I. M. Gonçalves, N. F. F. de Soares, R. F. Teófilo, *J. Chemom.* **2020**, *34*, e3193.
[21] G. Derringer, R. Suich, *J. Qual. Technol.* **1980**, *12*, 214.
[22] J. Schiller, R. Süß, B. Fuchs, M. Müller, M. Petković, O. Zschörnig, H. Waschipky, *Eur. Biophys. J.* **2007**, *36*, 517.
[23] S. Bourcier, S. Bouchonnet, Y. Hoppilliard, *Int. J. Mass Spectrom.* **2001**, *210-211*, 59.
[24] P. J. A. Madeira, M. H. Florêncio, *J. Mass Spectrom.* **2009**, *44*, 1105.
[25] M. Niehaus, J. Soltwisch, *Sci. Rep.* **2018**, *8*, 7755.

[26] A. Teearu, S. Vahur, U. Haljasorg, I. Leito, T. Haljasorg, L. Toom, *J. Mass Spectrom.* **2014**, *49*, 970.
[27] M. A. Butt, *Coatings* **2022**, *12*, 1115.
[28] Q. Zhang, Y. Li, P. Sui, X.-H. Sun, Y. Gao, C.-Y. Wang, *Talanta* **2024**, *266*, 125022.
[29] C. C. Shafer, J. Di Lucente, U. R. Mendiola, I. Maezawa, L.-W. Jin, E. K. Neumann, *J. Am. Soc. Mass Spectrom.* **2024**, *35*, 2554.
[30] R. J. Maganti, X. L. Hronowski, R. W. Dunstan, B. T. Wipke, X. Zhang, L. Jandreski, S. Hamann, P. Juhasz, *J. Histochem. Cytochem.* **2019**, *67*, 203.
[31] S. N. Jackson, H.-Y. J. Wang, A. S. Woods, *Anal. Chem.* **2005**, *77*, 4523.
[32] D. Leontyev, A. N. Pulliam, X. Ma, D. A. Gaul, M. C. LaPlaca, F. M. Fernandez, *Front. Chem.* **2024**, *12*, 1394064.
[33] A. Li, L. Xu, bioRxiv. **2023**.
[34] S. M. Bernard, D. Z. Habash, *New Phytol.* **2009**, *182*, 608.
[35] B. G. Forde, P. J. Lea, *J. Exp. Bot.* **2007**, *58*, 2339.
[36] L. Wang, X. Pan, L. Jiang, Y. Chu, S. Gao, X. Jiang, Y. Zhang, Y. Chen, S. Luo, C. Peng, *Front. Nutr.* **2022**, *9*, 943911.
[37] W. Sun, M. H. Shahrajabian, S. A. Petropoulos, N. Shahrajabian, *Plants* **2023**, *12*, 2469.
[38] L.-Q. Chen, L. S. Cheung, L. Feng, W. Tanner, W. B. Frommer, *Annu. Rev. Biochem.* **2015**, *84*, 865.
[39] T. Tufail, H. B. U. Ain, S. Noreen, A. Ikram, M. T. Arshad, M. A. Abdullahi, *Food Sci. Nutr.* **2024**, *12*, 8715.
[40] J. Kokesch-Himmelreich, O. Wittek, A. M. Race, S. Rakete, C. Schlicht, U. Busch, A. Römpp, *Food Chem.* **2021**, *385*, 132529.
[41] M. Maia, A. McCann, C. Malherbe, J. Far, J. Cunha, J. Eiras-Dias, C. Cordeiro, G. Eppe, L. Quinton, A. Figueiredo, E. De Pauw, M. S. Silva, *Front. Plant Sci.* **2022**, *13*, 1012636.
[42] D. Sturtevant, Y.-J. Lee, K. D. Chapman, *Curr. Opin. Biotechnol.* **2016**, *37*, 53.
[43] H. Enomoto, *Molecules* **2020**, *25*, 4600.
[44] H. Enomoto, K. Sato, K. Miyamoto, A. Ohtsuka, H. Yamane, *J. Agric. Food Chem.* **2018**, *66*, 4958.
[45] J. Wang, E. Yang, P. Chaurand, V. Raghavan, *Food Chem.* **2021**, *345*, 128838.
[46] D. Milosavljević, V. Maksimović, J. Milivojević, I. Djekić, B. Wolf, J. Zuber, C. Vogt, J. D.šić Maksimović, *Plants* **2023**, *12*, 2238.
[47] I. Urün, S. H. Attar, D. A. Sönmez, M. A. Gündeşli, S. Ercişli, N. E. Kafkas, L. M. Bandić, B. Duralija, *Plants* **2021**, *10*, 1654.
[48] D.-S. Kim, K.-J. Park, J. H. Choi, J.-H. Lim, H.-J. Kim, *Sci. Hortic.* **2023**, *321*, 112283.
[49] J. Luo, W. Chen, Y. Pan, Q. He, J. Sun, W. Bai, *Food Chem.* **2025**, *464*, 141740.
[50] D. Veličković, G. Zhang, D. Bezbradica, A. Bhattacharjee, L. Paša-Tolić, K. Sharma, T. Alexandrov, C. R. Anderton, *J. Am. Soc. Mass Spectrom.* **2020**, *31*, 508.
[51] J. G. Swales, G. Hamm, M. R. Clench, R. J. A. Goodwin, *Int. J. Mass Spectrom.* **2019**, *437*, 99.
[52] T. Mahamdi, C. G. Serna, R. Giné, J. Rofes, S. A. Mohammed, P. Ràfols, X. Correig, M. García-Altares, C. Hopf, S.-A. Iakab, O. Yanes, *J. Am. Soc. Mass Spectrom.* **2025**, *36*, 1100.

Manuscript received: July 3, 2025
Revised manuscript received: September 20, 2025
Version of record online: